Elevated glucose alters global gene expression and tenascin-C alternative splicing in mesangial cells

Maria E. Vega [1], John B. Finlay [1], Mansi Vasishtha and Jean E. Schwarzbauer

Department of Molecular Biology, *Princeton University, Princeton, NJ 08544, USA*

Correspondence to Jean E. Schwarzbauer: *jschwarz@princeton.edu.*
https://doi.org/10.1016/j.mbplus.2020.100048

Abstract

Mesangial cells are the major extracellular matrix (ECM)-producing cells in the kidney glomerulus and, when exposed to elevated glucose levels, they up-regulate assembly of fibronectin (FN) and other ECM proteins. Increases in glucose concentration are known to alter gene expression; here we investigated the connection between increased ECM production and changes in gene expression in mesangial cells. Comparison of mesangial cells grown in normal or high glucose conditions by RNA-sequencing showed significant expression changes in over 6000 genes and, when grouped by KEGG pathway analysis, identified the ECM-receptor interaction and focal adhesion pathways among the top 5 upregulated pathways. Of note was the significant increase in expression of tenascin-C (TN-C), a known regulator of FN matrix assembly. Mouse TN-C has multiple isoforms due to alternative splicing of 6 FNIII repeat exons. In addition to the transcriptional increase with high glucose, exon inclusion via alternative splicing was also changed resulting in production of higher molecular weight isoforms of TN-C. Mesangial cells grown in normal glucose secreted small isoforms with 1–2 variable repeats included whereas in high glucose large isoforms estimated to include 5 repeats were secreted. Unlike the smaller isoforms, the larger TN-C was not detected in the FN matrix. This change in TN-C isoforms may affect the regulation of FN matrix assembly and in this way may contribute to increased ECM accumulation under high glucose conditions.

Introduction

Diabetes is a chronic disease on the rise worldwide [1]. In diabetes patients, chronic elevation of blood glucose leads to additional complications [2], such as diabetic nephropathy, the leading cause of end-stage renal failure in the United States [3]. A key histological feature of diabetic nephropathy is the progressive loss of the filtration capabilities of the kidney glomeruli due to accumulation of extracellular matrix (ECM) [4]. Excess amounts of the ECM proteins fibronectin (FN) and type IV collagen can be detected in renal biopsies of patients with diabetic nephropathy [5], and cultured mesangial cells, the major ECM-producing cells in the glomerulus, increased assembly of FN and collagen fibrils when exposed to elevated glucose levels [6]. Using a mouse mesangial cell model, we have previously described several glucose-dependent mechanisms for excessive FN matrix assembly including increases in activity of integrin receptors for FN [6], cell interactions with advanced glycation end products [7], and increased lysine acetylation [8]. In addition to ECM-specific effects of glucose, others have identified roles for epigenetic changes in various diabetic animal and cell models of diabetic nephropathy [9,10]. For example, elevated glucose levels altered gene expression by increasing activating histone marks while reducing repressive histone marks in both in vivo and cell culture models [11,12]. Glucose-mediated modulation of histone methylation has also been linked to TGF-β-dependent promoters and expression of ECM-associated genes [13]. mRNA profiling by microarray analyses of mesangial and other cell types treated with elevated glucose conditions has shown changes in expected

pathways like cell proliferation and metabolism, but also in pathways related to the cytoskeleton and focal adhesions [14,15]. The effects of glucose levels even extend to changes in alternative splicing of certain transcripts, including growth factors, their receptors, and FN [16–19]. Clearly, changes in glucose concentration can affect a wide range of intracellular processes leading to alterations in cell structures and functions.

In this study, we used an unbiased approach to identify mesangial cell gene expression changes that coincide with increases in FN matrix assembly induced by exposure to high glucose levels. RNA-sequencing analyses were applied to mesangial cells grown in either normal (5 mM) or high (30 mM) glucose conditions. Our results show that genes related to ECM proteins, their receptors and focal adhesion proteins were among the most upregulated. ECM proteins including tenascin-C (TN-C) were significantly upregulated more than 2-fold. TN-C protein structure varies by alternative splicing and we show changes in splicing that result in secretion of distinct TN-C isoforms in normal and high glucose conditions. Because TN-C is well-known for its ability to modulate cell-ECM interactions, our findings raise the possibility that isoform changes in the diabetic kidney may allow excess ECM accumulation.

Materials and methods

Cell culture

Conditionally immortalized mesangial cells, isolated from an immortomouse expressing interferon-inducible, temperature-sensitive SV40 large T antigen, were maintained at 33 °C in DMEM containing: 10% fetal bovine serum (FBS, Hyclone), 100 IU/ml interferon-γ, 20 mM glucose, 10 mM mannitol, 1 mM sodium pyruvate, 100 U/ml penicillin, 100 µg/ml streptomycin and 0.25 µg/ml amphotericin B [20]. Cells were differentiated into a phenotype similar to freshly isolated primary mesangial cells by altering the culture temperature to 37 °C and removing interferon-γ for 4 d. Cells were then re-plated and serum starved for 20 h in medium without FBS or interferon-γ but containing 5 mM glucose and 25 mM mannitol. After starvation, cells were conditioned for 24 h in media with serum and either 5 mM glucose plus 25 mM mannitol or 30 mM glucose and then re-plated for experiments. After 24 h of conditioning, mesangial cells were plated for an additional 48 h in either 5 mM or 30 mM glucose for a total 72 h growth before analysis. Baby hamster kidney (BHK) cell lines expressing human TN-C that contains seven of the variable FNIII repeats (HxB.L, large isoform) or none of the variable repeats (HxB.S, small isoform) were kindly provided by Harold Erickson (Duke University School of Medicine [21]). BHK cells were grown in DMEM with 10% heat-inactivated FBS plus antibiotics and antimycotic as above.

RNA isolation and RNA-sequencing

Cells were lysed with TRIzol reagent (Invitrogen), lysates were homogenized with a 20 g needle, and RNA was isolated according to the manufacturer's instructions. After chloroform addition and centrifugation, the aqueous layer was loaded onto a Qiagen RNeasy column and RNA was purified as instructed, including treatment with DNase (New England Biolabs). RNA was quantified using Nanodrop, only samples with a 260 nm/280 nm ratio of 2 ± 0.15 and a 260 nm/230 nm > 1.95 were considered for submission for RNA-seq analysis. RNA quality of submitted samples was verified by analyzing integrity of 18S and 28S rRNAs by electropherogram. All samples had an RNA integrity number > 9.8.

RNA samples from two separate biological replicates for each condition (5 mM glucose, 30 mM glucose) were submitted to the Genomics Core Facility at the Lewis Sigler Institute for Integrative Genomics (Princeton University). RNA samples were used to create a cDNA directional library, samples were then run on an Illumina Hi-Seq 2000 sequencer in one, 8-lane reaction. 75 nucleotide single-end reads were performed for each sample. Reads were de-multiplexed using a barcode-splitter program by Parsons and Leach Copyright, 2017 (Princeton University). FastQC was run on each sample to check for quality of reads [22]. No trimming was necessary. Reads were mapped to genes using TopHat2 [23]. The *Mus musculus* Ensembl genome was used as the reference genome, and default settings were used [24]. Gene body coverage was used to assess 5′ to 3′ bias [25]; no bias was present. The number of reads per gene was determined with htseq-count [26]. The program was run in union mode with a minimum alignment quality of 10. All further data analysis was conducted with DESeq2. Adjusted *p*-values were calculated by Benjamini and Hochberg method [27]. *P*-values were used to rank differentially expressed genes and changes in expression for specific genes were confirmed by qPCR. Kyoto Encyclopedia of Genes and Genomes (KEGG) pathway analysis was conducted using Pathview [28]. Only genes with adjusted *p*-values <0.05 between conditions or those with expression levels of 0 were input into Pathview for analysis.

Reverse transcription and quantitative PCR (qPCR)

RNA isolated from mesangial cells was used for reverse transcription reactions. 1 µg of total RNA was reversed transcribed using random hexamer primers and Superscript II reverse transcriptase (Invitrogen) for 1 h at 37 °C. qPCR reactions were

performed in a mix containing Power SYBR Green PCR Master Mix (Applied Biosystems) and 400 nM of each primer on the Mx3000P QPCR System (Agilent Technologies) in a 25 µl final reaction volume. PCR reaction conditions were: 10 min at 95°, followed by 40 cycles of 15 s at 95°, 30 s at 55°, and 30 s at 72°. Data analysis was performed using MxPro TM QPCR software (Agilent Technologies). Data are expressed as mean fold change in gene expression relative to GAPDH control. In Fig. 4A, data for all reactions from a given primer pair were normalized to the value for one of the 5 mM reactions from that pair. Resulting values were averaged separately for 5 mM and 30 mM samples. Statistical significance of comparisons between averages from 5 mM or 30 mM glucose samples was determined by the one-way ANOVA with $p < 0.05$ as statistically significant.

Primers were designed using Primer-Blast and IDT Oligo Analyzer. DNA samples were run on a polyacrylamide gel to confirm sole amplification of the correct DNA fragment. Melting curve analysis showed one peak for each reaction, confirming that only one product was amplified.

qPCR primers for ECM genes

Gene	Forward 5′-3′	Reverse 5′-3′
Fn1	AAGGCTGGATGA TGGTGGACTG	TGAAGCAGGTTTC CTCGGTTG
Tnc	GAGGAACGTCAA GGCAGACA	CCGTAAGTCCTTG GGTGCAT
Npnt	CACGAGTAATTAC GGTTGACAACAG	CTGCCGTGGAATG AACACAT
GAPDH	AATGGTGAAGGT CGGTGTGAA	CCGTGAGTGGAGT CATACTGG

qPCR primers for TNC alternative exon junctions

Primer pair	Forward 5′-3′	Reverse 5′-3′
III5 - A1	CAGGGCAAGAATA CACTGTTCTCC	CCAGTTGAGTCT GAGGCCAT
A1 - A2	CCAGGCCTCAAG GTTGCC	GTCGTGTCAGCC TCTAGCAC
A2 - A4	GCCTGGGCTCAA AGCAGC	TCCAGTTGAGTGT GAGGCCG
A4 - B	GGCCTCAAGGCC GACAC	CATGTCGAAGATC CCGTCGG
B - C	CATGTCGAAGATC CCGTCGG	CCAGGAAACTGTG AACCCGT
C - D	GGCCTCATAACTG GCATTGG	TCAGCAGTCCAGG ACAGACG
D - III6	CCAGGGACATAAC AGGTCTCAG	GGAAACTCTCCACCT GAGCAG

PCR for cloning and sequencing of Tnc splice variants

Primers were designed within the flanking FNIII repeat exons (III5 and III6) or within each of the alternatively spliced exons. PCR reactions containing forward and reverse primers and cDNA prepared as above from 5 mM and 30 mM glucose samples were run with the following cycle conditions: 35 cycles of 95 °C 30 s, 60 °C 30 s, 72 °C 130 s. Products were analyzed on a 1.5% agarose-TAE gel with a 100 base pair ladder (NEB). The gel was stained with ethidium bromide and imaged using Bio-Rad gel doc.

TNC PCR primers

Primer pair	Forward 5′-3′	Reverse 5′-3′
III5 - III6	CAACTACAGCCTC CCCACAG	TCCGGAAACTCTC CACCTGA
A1 - D	CTCACAACTTCACA GTACCTGG	AAGGGAGGGATAT TTCTTGT
A1 - A2	CTCACAACTTCACA GTACCTG	TTCTGGACAGTCT GGGTCGT
A2 - A4	CTGTCCAGAACCTC ACAGTC	GGGATGTCCACA GCTCTGA
A4 - B	TCAGAGCTGTGGAC ATCCCA	TTCAGCACCAGATA TATTATG
B - C	AAACAGCAGAACAT AATATATCT	TGGGTTCCTGAAAG TGTGAA
C - D	TTCACACTTTCAGG AACCCA	AAGGGAGGGATATT TCTTGT

Bands of interest were isolated using Monarch DNA gel isolation kit (NEB). Purified PCR products were cloned into the pGEM-T vector (Promega) following manufacturer's instructions. Bacterial colonies were screened by colony PCR using T7 and SP6 primers to amplify inserts which were analyzed by agarose gel electrophoresis as above. Colonies with expected size of PCR product were used for plasmid extraction using QIAprep Spin Miniprep Kit (Qiagen) and plasmids were then submitted for sequencing.

Immunoblotting

Conditioned medium was collected from cells before cell lysis and stored with addition of 10 mM EDTA, 2 mM PMSF at –20 °C. Cells were lysed in deoxycholate (DOC) buffer, DOC-soluble cell lysate was separated from DOC-insoluble matrix by centrifugation, and the insoluble pellet was solubilized in SDS buffer with boiling [29–31]. Total protein concentration of the DOC-soluble fraction was measured using BCA assay (Pierce). Equal amounts of DOC-soluble protein or proportional volumes of

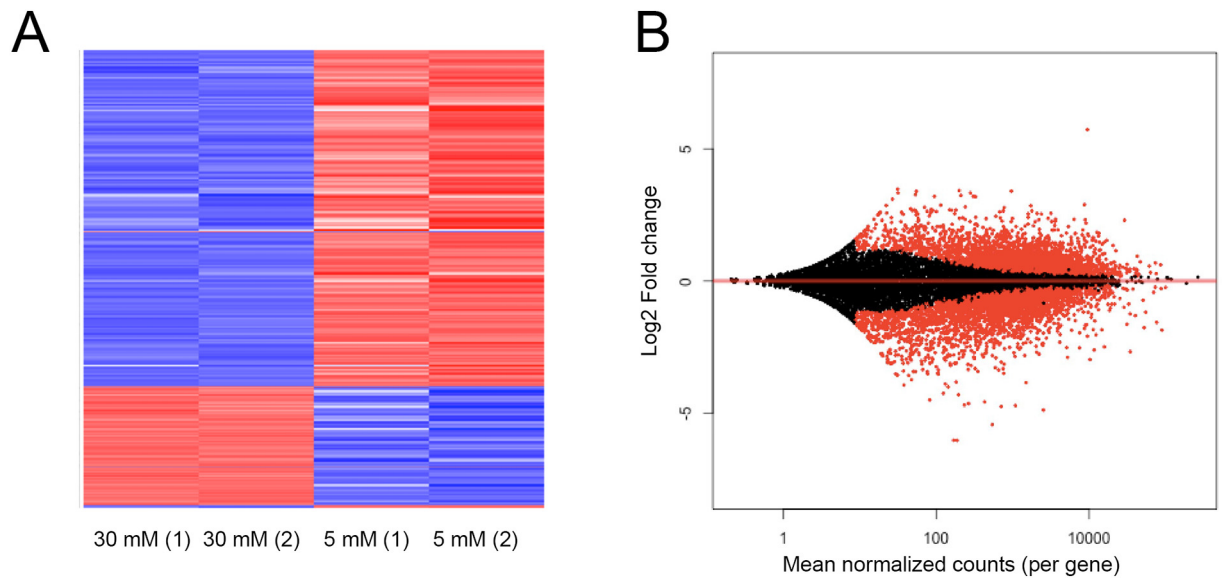

Fig. 1. Gene expression changes with culture in elevated glucose conditions. RNA from mesangial cells grown in 5 mM or 30 mM glucose for 72 h was used for RNA-sequencing analysis. (A) A heat-map of the top 1000 most significantly changed genes was generated for two biological replicates (1 and 2) of each glucose condition (30 mM and 5 mM) (see also Supplementary Table 1). Red indicates that expression is higher and blue indicates that expression is lower in the 30 mM compared to the parallel 5 mM sample. (B) An MA plot shows the relationship between normalized gene expression and $\log_2$-fold change in glucose conditions. Each dot represents a gene, and all red dots are statistically significant changes. 5 mM was the baseline condition used to calculate the $\log_2$-fold change. For (A) and (B), statistical significance was determined by a Wald test and subsequently adjusted to correct for high sample number (p-value adjusted). An adjusted p-value cutoff of $p < 0.05$ was used.

DOC-insoluble material were separated by SDS-PAGE on 5% (for TN-C) or 10% (for GAPDH) polyacrylamide gels. For conditioned medium, 10 µl for each condition were separated by SDS-PAGE on a 5% gel. Gels were transferred to a nitrocellulose membrane and immunoblotted as described [29]. The following antibodies were used: for TN-C - R759 rabbit polyclonal antiserum at 1:10,000 and for GAPDH - Cell Signaling (14C10) rabbit monoclonal antibody at 1:5000. (R759 was generated in-house.) Secondary HRP-conjugated antibodies (Thermo-Fisher Scientific) were used at 1:10,000 dilution. All antibody incubations were for 1 h. SuperSignal West Pico Plus ECL reagent (Pierce) was used to develop blots. Densitometry was performed on scanned films using Adobe®Photoshop®Software, and exposures yielding signals within the linear range were quantified. TN-C levels in conditioned medium were normalized to the total protein in DOC-soluble lysates. Fold-change and SEM were calculated from the means of three independent experiments.

Immunofluorescence microscopy

Differentiated mesangial cells in either 5 mM or 30 mM glucose medium with 10 µg/ml human plasma FN were fixed with 3.7% formaldehyde in PBS and incubated with anti-TN-C (R759 rabbit polyclonal antiserum diluted 1:100) or anti-human FN (mouse monoclonal concentrated supernatant HFN7.1 diluted 1:100, DSHB, Iowa) followed by Alexa-Fluor-488- or 568-conjugated goat anti-rabbit or goat anti-mouse IgG (Invitrogen) antibody (1:600) [8]. Samples were mounted in ProLong Gold antifade reagent (LifeTechnologies). A Nikon Eclipse Ti microscope and Hamamatsu C10600 ORCA-R2 digital camera were used to capture images. Mean fluorescence measurements were performed using ImageJ on 6 randomly selected fields per condition. Background fluorescence was removed from images using a rolling ball radius of 50. Representative fields are shown. Images were adjusted equally using Adobe®Photoshop® software.

Results

Effects of glucose concentration on global gene expression patterns in mesangial cells

To identify the effects of glucose levels on global gene expression, RNA was analyzed from mesangial cells grown in medium containing either 5 mM (normal) or 30 mM (high) glucose for 72 h. We have previously established that mesangial cells increase

FN and collagen IV matrix assembly with higher glucose concentration [6]. RNAs from two independent cultures for each glucose concentration were submitted for Illumina RNA-sequencing. Data analysis identified significant changes in over 6000 genes (Supplementary Table 1). Clustering of the top 1000 significantly-changed genes shows consistent patterns of up- and down-regulation of expression in biological replicates from 5 mM and from 30 mM conditions (Fig. 1A). Importantly, profiles of up- and down-regulated genes differed significantly between 5 mM and 30 mM glucose conditions, demonstrating that glucose concentration affects mesangial cell gene expression. An MA plot, which graphs the relationship between normalized gene expression, extent of $\log_2$-fold change, and statistical significance (red dots), shows widespread increases and decreases in gene expression levels between the high and normal glucose conditions (Fig. 1B).

In order to visualize potential connections between gene products significantly altered under elevated glucose conditions, we used the Pathview program to sort up-regulated and down-regulated genes into biological pathways. Genes with adjusted p-values <0.05 were assigned to KEGG pathways and then each of the 523 KEGG pathways was assigned a degree of change depending on how many nodes within the pathway were significantly up- or down-regulated. 46 pathways were significantly changed ($p < 0.05$) in the mesangial cells grown in 30 mM glucose. Among these, 38 were up-regulated, and 8 were down-regulated compared to 5 mM conditions. Two of the most upregulated KEGG pathways are ECM-receptor interaction and focal adhesion (Table 1). Also, within this list of pathways were those known to respond to changes in glucose levels and metabolism including the citric acid cycle, glycolysis, and the cell cycle including oocyte meiosis in which many of the nodes overlap with cell cycle genes (Table 1).

Table 1. Statistically significant KEGG pathways. Pathview program output for top KEGG pathways that were up-regulated in 30 mM glucose conditions. Only pathways with greater than 2-fold increase are shown. Pathways are sorted by degree of up-regulation, from highest to lowest. Pathways highlighted in yellow are discussed in the text.

KEGG Pathway	Degree of up-regulation	p-value
Oocyte meiosis	3.556	9.429E-07
ECM-receptor interaction	3.434	2.938E-06
Focal adhesion	3.093	1.790E-05
Progesterone-mediated oocyte maturation	3.022	3.252E-05
Glycolysis/Gluconeogenesis	2.971	5.790E-05
Tight junction	2.924	5.527E-05
Regulation of actin cytoskeleton	2.886	5.714E-05
Circadian entrainment	2.617	2.819E-04
Gap junction	2.571	4.181E-04
Cell cycle	2.538	4.178E-04
Ubiquitin mediated proteolysis	2.288	0.0014
Hippo signaling pathway	2.232	0.0018
mRNA surveillance pathway	2.144	0.0029
Long-term depression	2.135	0.0031
Endocrine and other factor-regulated calcium reabsorption	2.127	0.0032
Vasopressin-regulated water reabsorption	2.098	0.0041
Pentose phosphate pathway	2.096	0.0043
Leukocyte transendothelial migration	2.050	0.0044
Adherens junction	2.041	0.0049
Melanogenesis	2.008	0.0051
Chemokine signaling pathway	2.006	0.0048

Up-regulation of ECM-related genes and pathways

The ECM-Receptor Interaction Pathway shows many up-regulated ECM proteins and their receptors (Supplementary Fig. 1). Because the KEGG pathway nodes do not distinguish between different protein family members, we have listed those family members with a significant adjusted p-value <0.05 in Table 2. Among these genes, three ECM genes (encoding tenascin-C, collagen VI, nephronectin) and two integrin genes (Itgb6, Itga1) had a $\log_2$-fold change greater than 1.5 and also had very low adjusted p-values, suggesting strong up-regulation in response to high glucose. Collagen IV (Col4) was significantly up-regulated with a change of 1.48, corresponding with our previous data [32]. Up-regulation of nephronectin (Npnt) expression is noteworthy because this protein is a reliable diagnostic for diabetic nephropathy compared to other glomerular diseases in human kidney tissue specimens [33]. Thus, the increase in Npnt gene expression serves as a validation of our mesangial cell model. Both Npnt and Col6 RNA levels were quite low even after up-regulation by glucose stimulation (~10-fold and ~4-fold less than Tnc, respectively). The low level of Npnt expression in particular made it difficult to detect the protein and therefore we did not analyze these genes further.

In addition to overall changes in ECM related genes, the RNA-sequencing data provided information about relative expression levels of ECM proteins and their receptors. Fibronectin (Fn1) and integrin β1 (Itgb1) are two of the most highly expressed genes, independent of glucose concentration (Supplementary Table 2). In high glucose conditions, Fn1 expression was about 4-fold higher than Tnc. RNA-sequencing counts show significant up-regulation of Tnc and Npnt (Fig. 2A), but no significant change in Fn1 gene expression (Fig. 2A), which confirms our previous study [6]. We validated the RNA-sequencing results by quantitative PCR (qPCR), which showed significant up-regulation of the relative levels of Tnc (3.0-fold) and Npnt (3.3-fold), and no significant changes in Fn1

Table 2. Changes in ECM and integrin genes. RNA-sequencing data for genes identified within the ECM-Receptor Interaction KEGG Pathway are listed. Only genes with an adjusted p < 0.05 are shown. Genes highlighted in yellow are discussed in the text.

Category	KEGG Gene Node	Gene	5mM 1 counts	5mM 2 counts	30mM 1 counts	30mM 2 counts	Log_2 fold change	Adjusted p-value
ECM Proteins	Collagen	Col1a1	139.56	189.20	351.10	540.38	1.332	1.07E-04
		Col4a6	711.23	799.35	1973.14	2322.61	1.480	6.87E-19
		Col6a1	352.93	567.61	3000.33	3176.80	2.653	8.83E-34
		Col9a3	59.05	74.23	8.71	7.55	-2.199	1.92E-04
	Laminin	Lamb3	3357.55	3026.32	5223.02	5803.16	0.782	7.04E-10
	Thrombospondin	Thbs1	4651.19	5125.65	12906.66	14621.17	1.480	5.46E-37
	Osteopontin	Spp1	4162.72	4195.03	7307.39	7538.40	0.824	8.33E-17
	Tenascin	Tnc	4157.35	4623.22	12334.06	13650.34	1.552	2.94E-42
	Nephronectin	Npnt	245.58	309.60	1036.87	1419.74	2.061	1.48E-17
	Von willebrand factor	Vwf	33.55	50.70	9.67	4.20	-1.614	0.016
	Agrin	Agrn	10920.76	12185.86	17156.65	19719.50	0.668	5.20E-08
	Perlecan	Hspg2	16947.45	18739.12	21932.81	23006.22	0.330	0.002
ECM Receptors	Integrins	Itga1	96.62	141.22	388.82	391.86	1.60	5.83E-07
		Itga3	8155.01	9651.10	11453.88	10908.19	0.33	0.014
		Itga5	3248.85	3859.17	6621.63	6920.83	0.92	1.63E-12
		Itga6	3046.22	2685.04	4170.68	4385.09	0.57	1.04E-05
		Itga7	397.22	435.44	634.50	700.64	0.66	0.003
		Itgav	7767.19	8346.60	9502.99	9261.89	0.22	0.050
		Itgb1	29560.41	27853.40	36053.33	42444.62	0.45	2.46E-04
		Itgb3	220.08	192.82	491.35	518.56	1.24	9.08E-07
		Itgb5	3267.64	3811.19	6055.80	6866.29	0.86	4.17E-10
		Itgb6	267.05	358.49	1101.67	1354.29	1.90	1.52E-16
		Itgb7	1947.17	1791.53	865.67	977.54	-1.00	2.05E-10

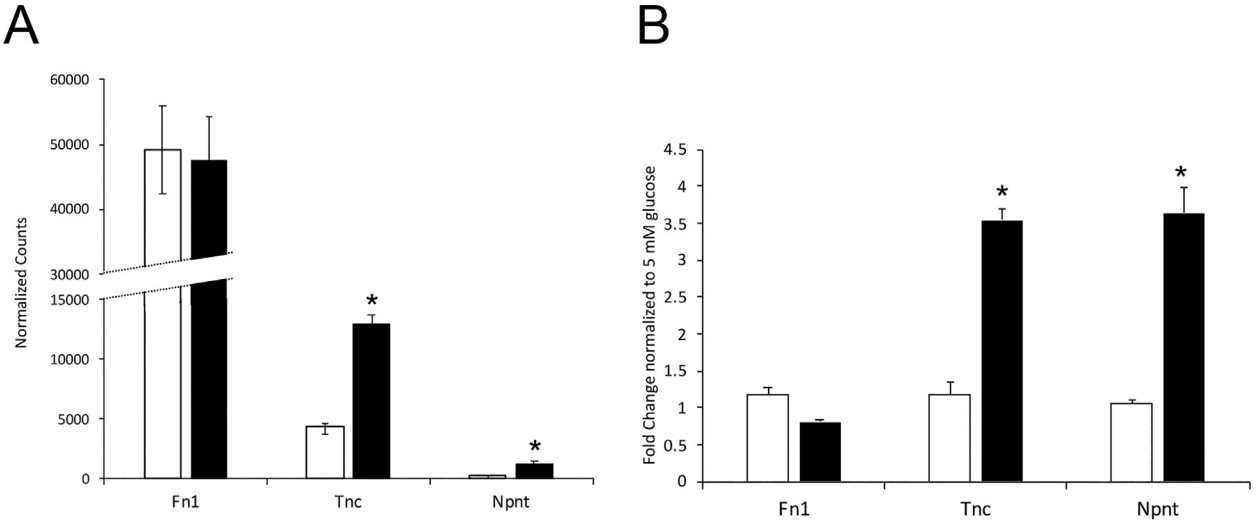

Fig. 2. Up-regulation of Tnc and Npnt but not Fn1 gene expression. (A) Normalized counts from RNA-sequencing data were averaged for biological duplicates grown in 5 mM (white bar) or 30 mM (black bar) glucose. Data are shown in Supplementary Table 1. Statistical significance was determined with a Wald test and adjusted *p*-values were used, * $p < 0.05$. (B) Quantitative PCR (qPCR) analysis was performed using RNAs from mesangial cells grown in 5 mM (white bar) or 30 mM (black bar) glucose for 72 h. The graph represents mean fold-change ± SEM (n = 3) and one-way ANOVA was performed to determine significance, *$p < 0.05$.

(Fig. 2B). Together, our results show that Tnc, Npnt, and Col6 are the most up-regulated ECM genes in response to elevated glucose levels with Tnc being the most highly expressed of the three. Fn1 on the other hand is highly expressed independent of glucose concentration.

Identification of alternatively spliced Tnc mRNAs in mesangial cells

The effects of TN-C as a modulator of cell-FN interactions are well-established [34,35]. TN-C binds directly to FN [36–38] and reduces FN-mediated signaling through syndecan-4 resulting in changes in cell proliferation, contractility, and FN matrix assembly [39–41]. The Tnc transcript is alternatively spliced and splicing patterns can affect TN-C binding to FN [38]. The mouse Tnc transcript contains 6 exons encoding FNIII repeats that can be included or skipped by alternative splicing (Fig. 3A). At least 29 different combinations of these exons have been reported in mouse tissues and cell lines and at different developmental stages [40]. To determine whether all six of the alternatively spliced FNIII exons could be detected in Tnc mRNAs from mesangial cells, PCR reactions were performed using primers from adjacent repeats. Products the length of a single exon (~270 bp) and spanning the junction

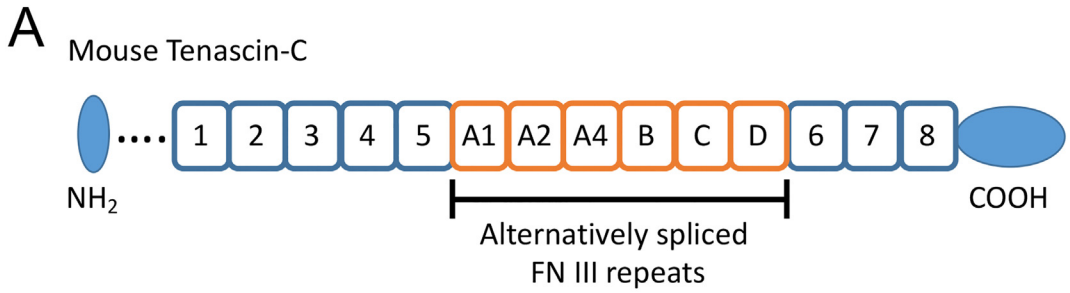

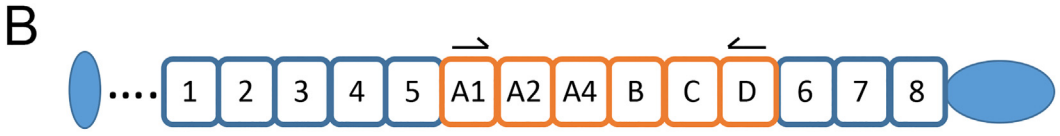

# of FN III repeats	Sequences Identified
2	A1+D
3	A1+C+D
4	A1+B+C+D; A1+A4+B+D
5	A1+A2+A4+B+D
6	A1+A2+A4+B+C+D

# of FN III repeats	III5 - B Sequences Identified	A4 - III6 Sequences Identified
2	A4+B	A4+B
3	A1+A4+B	A4+B+D
4	A1+A2+A4+B	A4+B+C+D

Fig. 3. PCR products within the alternatively spliced region. (A) Schematic of mouse TN-C showing FNIII repeats (squares), with constitutive repeats outlined in blue and variable exons shown as orange squares. (B) PCR primers were designed within the first and last variable TN-C exons A1 and D (black arrows). (C) PCR primers III5 - B (black arrows) and A4 - III6 (green arrows) were used to amplify within the variable region. The numbers and combinations of repeats identified with various primer pairs are listed in the tables.

between exons were generated with all primer pairs (A1-A2, A2-A4, A4-B, B-C and C-D) using RNAs from both 5 mM and 30 mM glucose conditions (data not shown). Sequencing confirmed the amplification of the expected FNIII exon junctions. This analysis showed the presence of all alternatively spliced repeats but did not identify the combinations of exons that are included in Tnc mRNA. For that analysis, PCR primers were designed to amplify the regions between the constitutively included FNIII repeats (III-5 and III-6) that flank the alternatively spliced region, as well as between A1 and D, the first and last alternatively spliced repeats. Using III-5 to III-6 primers, we identified isoforms with no extra repeats, or with A1 only, D only, or A1 + D included (Table 3). Large PCR products with the III-5 to III-6 primer pair were visible by agarose gel electrophoresis but levels were too low to isolate for sequencing. We therefore used primers in A1 and D and the predominant PCR products were sequenced. Results are summarized in Fig. 3B and Table 3. Multiple products were obtained corresponding to the expected sizes ranging from inclusion of none, one, or more than one variable repeats between A1 and D. Internal primers were used to generate smaller PCR products in order to identify additional combinations of repeats (Fig. 3C, Supplementary Fig. 2, Table 3).

The list of repeat combinations in Table 3 includes the predominant PCR products from the various reactions. The most obvious feature is that in all but one product, A4 and B occur together. In this cohort of products, C is included less frequently than any other repeat but, when it is included, it is followed by D. This list is not meant to be comprehensive. Furthermore, we do not have information about the relative abundances of these products in RNAs from cells grown in 5 mM versus 30 mM media because the PCR reactions were performed for 40 cycles. However, this gross analysis allowed the identification of possible alternative exons that are included or excluded within Tnc mRNA in mesangial cells.

Table 3. Summary of alternatively spliced Tnc variants identified in mesangial cells. PCR reactions were performed with the listed primer pairs. The number of extra repeats included in a sequenced product is listed in column 2. The presence (+) or absence (blank) of an exon in the sequenced PCR product is marked.

Primers	Repeats	A1	A2	A4	B	C	D
III5 - III6	1	+					
	1						+
	2	+					+
III5 - A4	3	+	+	+			
III5 - B	3	+		+	+		
	4	+	+	+	+		
A1 - D	3	+				+	+
	4	+		+	+		+
	4	+			+	+	+
	5	+	+	+	+		+
	6	+	+	+	+	+	+
A2 - B	3		+	+	+		
A2 - D	4		+	+	+		+
A4 - III6	2			+	+		
	3			+	+		+
	4			+	+	+	+

Quantitative changes in alternative splicing of the Tnc transcript

In order to determine how alternative splicing is affected by growth in 30 mM glucose medium, we performed qPCR across each of the junctions between adjacent exons. The results show significant up-regulation of inclusion of all of the repeats in mesangial cells grown in higher glucose (Fig. 4A). Increases at 30 mM ranged between 1.9- and 2.8-fold compared to 5 mM RNA samples. However, this analysis does not illustrate the levels of individual repeats relative to the other variable exons. Therefore, we normalized the data to the 5 mM D-III6 product, which is the most abundant exon pair in both 5 mM and 30 mM glucose conditions (Fig. 4B). This analysis allowed us to directly compare relative levels of each junction. The low level of the C-D exon junction regardless of glucose conditions indicates that the C exon is included at the lowest frequency (Fig. 4B, Table 3). These results show that the alternatively spliced exons were not equally represented in the mesangial cell RNA population, but that inclusion of all exons was increased relative to GAPDH in high glucose conditions compared to normal glucose media.

Variations in TN-C isoform expression and matrix deposition with glucose

Mass spectrometry of TN-C isolated from conditioned medium of mesangial cells grown in 30 mM glucose conditions was used to determine the presence of alternatively spliced FNIII repeats. Peptides were scored with a peptide probability threshold of 95%. Unique peptides from each of the six FNIII repeats (A1, A2, A4, B, C, D) were identified in secreted TN-C (Supplementary Fig. 3). Mass spectrometry identifies short peptides, so we were not able to determine all of the possible combinations of alternative splicing of TN-C in mesangial cells. However, we did detect peptides across junctions between A1-A2, A1-A4, A4-B, A4-D, and B-D.

TN-C protein was analyzed in deoxycholate (DOC)-soluble lysates of mesangial cells. Surprisingly, different-sized bands predominated in cells grown under 5 mM or 30 mM glucose conditions for

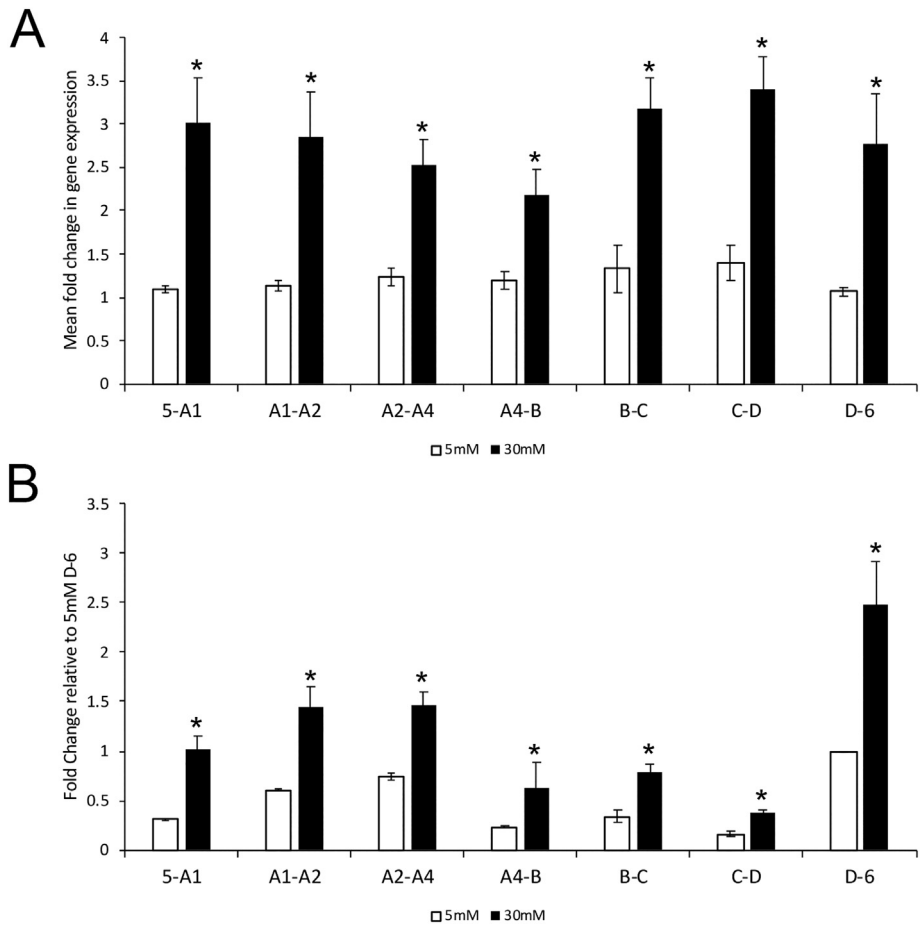

Fig. 4. Increased inclusion of variable repeats under 30 mM glucose conditions. RNA from mesangial cells grown in either 5 mM (white bars) or 30 mM (black bars) glucose was used for qPCR with primers from adjacent exons. (A) The fold-change in gene expression relative to GAPDH was determined for each pair of primers as described in Materials and Methods. Mean fold-change ± SEM for each junction: III5 - A1 (2.8 ± 0.5), A1 - A2 (2.5 ± 0.5), A2 - A4 (2.1 ± 0.2), A4 - B (1.9 ± 0.2), B - C (2.4 ± 0.1), C - D (2.4 ± 0.2) and D - 6 (2.6 ± 0.5). (B) All data from (A) were normalized to 5 mM glucose D - III6 mean fold change. Graphs represent mean fold-change ± SEM (n = 5) and one-way ANOVA was performed to determine significance, *$p < 0.05$.

72 h (Fig. 5A). While in normal glucose conditions the major band was ~240 kDa with a less intense band at ~290 kDa in the DOC-soluble cell fraction, in 30 mM glucose conditions the larger protein band was predominantly expressed. Sizes were determined using the 250 kDa molecular mass marker and recombinant tenascins HxB.S at 220 kDa (with no variable repeats) and HxB.L at 320 kDa (with 7 variable repeats) (Supplementary Fig. 4) [21]. The average size of one variable repeat calculated from the difference in size between HxB.S and HxB.L is 14.3 kDa. This size estimate includes contributions from potential N-linked glycosylation at sites in all but the D repeat. From this size calculation, we estimate that the ~240 kDa band in mesangial cell lysates contains 1–2 extra repeats and that the ~290 kDa band has 5 extra repeats. These differences in molecular weight indicate that increased inclusion of some FNIII exons detected by qPCR leads to a change in the TN-C protein structure. Analysis of the DOC-insoluble fraction was used to identify proteins incorporated into the ECM. The smaller TN-C band was detected in the DOC-insoluble fraction from mesangial cells grown in 5 mM glucose medium, but TN-C was undetectable in 30 mM conditions (Fig. 5A). Small but not large TN-C was also incorporated into BHK-HxB DOC-insoluble matrix (Supplementary Fig. 4) as previously reported by Erickson's group [21,36].

To correlate increased Tnc mRNA expression with increased protein levels, we analyzed mesangial cell conditioned medium which contained higher levels of TN-C when cells were cultured in 30 mM glucose medium compared to 5 mM glucose medium (Fig. 5B). Quantification showed an average of 3.3-fold more TN-C in high glucose conditions. TN-C

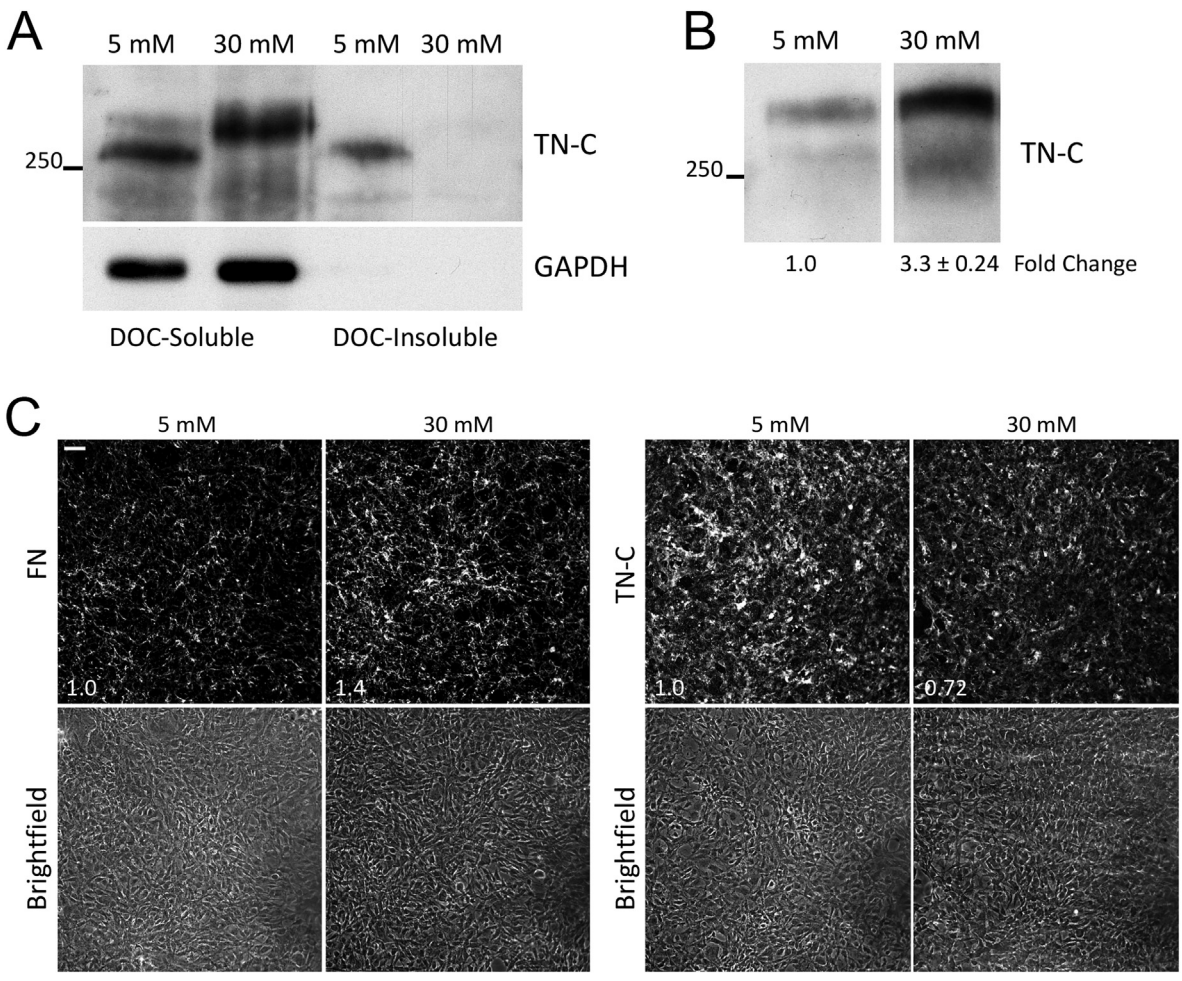

Fig. 5. Expression and localization of TN-C splice isoforms. (A) DOC-soluble and DOC-insoluble fractions were isolated from lysates of mesangial cells grown in 5 mM or 30 mM glucose media. Fractions were immunoblotted with anti-TN-C antiserum or GAPDH as indicated. Representative blots are shown from three independent experiments. (B) Equal volumes of conditioned media collected from mesangial cells grown in 5 mM or 30 mM glucose for 72 h and cells were then lysed in DOC buffer. Conditioned media were immunoblotted with anti-TN-C antibodies. Representative results are shown and these samples are from the same blot and exposure time. Band intensity values were normalized to the total protein in parallel DOC-soluble lysates and then used to calculate the average fold change between 5 and 30 mM TN-C levels (mean ± SEM from three independent experiments). (C) Mesangial cells grown in either 5 mM or 30 mM glucose media with 10 µg/ml human FN were stained with anti-human FN or anti-TN-C antibodies. The mean fluorescence intensity of 6 randomly selected fields per condition was measured using Image J software. Representative images are shown for each condition. Scale bar = 50 µm.

is not present in serum (data not shown), allowing us to conclude that all protein in the conditioned medium is secreted by the mesangial cells.

Previous studies with fibroblasts have shown that alternative splicing can alter TN-C incorporation into a FN matrix, with smaller TN-C isoforms preferentially incorporated [36,42]. Staining of mesangial cells for TN-C also showed higher levels of fluorescence in 5 mM compared to 30 mM glucose conditions (Fig. 5C). Cell densities were equivalent as detected by phase microscopy, but, as we have reported previously [6,8], FN matrix levels were higher in 30 mM glucose cultures compared to 5 mM conditions (Fig. 5C). Taken together, our analyses of TN-C under elevated glucose conditions show increased expression and changes in splicing that affect TN-C deposition into a FN matrix.

Discussion

Increased accumulation of ECM proteins occurs when cells are exposed to high glucose conditions and could be related to corresponding epigenetic

changes [4,9]. In this study, we investigated the effects of growth in high glucose media on gene expression by mesangial cells. RNA-sequencing analyses comparing mesangial cells grown in normal or high glucose identified significant changes in over 6000 genes and up-regulation of ECM-receptor interaction and focal adhesion KEGG pathways. Of particular note was the increase in Tnc expression along with increased inclusion of alternatively spliced Tnc exons. Quantitative PCR analysis showed an overall stimulation of inclusion of variable exons under high glucose conditions and a corresponding shift to production of higher molecular weight TN-C isoforms. Moreover, unlike the smaller TN-C produced in normal glucose cultures, the larger splice isoforms were not detected in the mesangial cell FN matrix. Because TN-C acts as a negative regulator of cell-FN matrix interactions [34,39,41,43] and our findings show a shift toward an isoform that is not incorporated into the FN matrix, we propose that this change in TN-C may contribute to the accumulation of FN matrix in the diabetic glomerulus.

A regulatory relationship between TN-C and FN in the kidney has been shown in Habu snake venom-induced glomerulonephritis [44]. In wild type mice, the damaged glomeruli underwent a fairly typical wound healing response marked by cell proliferation, granulation tissue formation, and ECM remodeling. In TN-C knockout mice, the early wound healing response was reduced but FN and collagen IV accumulated uncontrollably later causing glomerulosclerosis and ultimately death [44]. In contrast to loss of TN-C, persistent TN-C expression during liver or lung damage is associated with excess deposition of ECM and fibrotic lesions [45,46]. A high level of TN-C has also been used as a diagnostic marker of fibrosis [47]. These phenotypes indicate that appropriate levels of TN-C have modulatory activity during ECM deposition in multiple tissues.

Many different factors have been linked to induction or repression of Tnc expression [35]. Stimuli include reactive oxygen species, mechanical stress, hypoxia, and even denatured collagen [48], and these stimuli can also be present with chronic elevation of glucose. Thus, it seems likely that the mechanism of Tnc upregulation is multifactorial. Along with Tnc, Col4 and Col6 RNAs were increased at least 1.5-fold in mesangial cells and these proteins have been implicated in diabetic nephropathy [49]. Collagen fibrillogenesis is downstream of FN matrix assembly, yet FN expression did not change with glucose concentration. Increased FN may not be needed since we found that, in normal glucose, Fn1 is already one of the most highly expressed genes in mesangial cells. Furthermore, in the mesangium, an exogenous supply of plasma FN is available through the continual exposure to blood.

Differences in alternative splicing of Tnc are a common phenomenon in developing tissues, during repair, and in disease [35]. In the mouse kidney, for example, a larger TN-C isoform dominates in the prenatal stage, while a smaller isoform takes over at birth [50] suggesting that they might play different roles in the developmental process. Higher matrix incorporation by recombinant TN-C lacking all variable repeats [21,37] and by small isoforms of mesangial TN-C (shown here) provide support for matrix-dependent functional differences resulting from splicing. TN-C binding by FN, contactin [51], and annexin II [52] can be affected by alternative splicing, and functional perturbation by antibody binding to variable repeats further implicates this region in protein interactions [35]. Large versus small TN-C isoforms also show differences in turnover by matrix metalloproteases [53] and in N-linked glycosylation sites. Alterations in binding activities, matrix incorporation, and protein stability are just some of the ways that the spliced region of TN-C might contribute to the regulation of ECM assembly. In contrast to numerous functional analyses of TN-C isoforms, much less is known about the mechanisms that control alternative splicing. One splicing factor, serine/arginine-rich (SR) protein SRSF6 [54,55], has been shown to increase the inclusion of variable exons in a skin hyperplasia model [56]. We did not detect a dramatic change in alternative splicing with siRNA knockdown of SRSF6 in mesangial cells (MEV, unpublished observations) but further analyses across the alternatively spliced region are needed.

Smaller isoforms of TN-C lacking most or all alternatively spliced repeats are incorporated into a FN matrix, whereas larger isoforms are not incorporated or are present at very low levels [36–38]. Small isoforms also bind to purified FN with higher affinity [36–38]. It has been hypothesized that in the absence of extra repeats, a secondary binding site on TN-C may be brought into close proximity to the main FN binding domain, and the resulting cooperativity makes the interaction significantly stronger [36]. TN-C binds to the primary heparin-binding domain of FN and, in so doing, prevents syndecan-FN interactions [39,41,43]. Engagement of α5β1 integrin together with syndecan-4 is needed for full activation of focal adhesion kinase (FAK) and Rho GTPase [42,57], allowing TN-C binding to FN to modulate both cell contractility and FN matrix assembly. Furthermore, the alternatively spliced region of TN-C promotes focal adhesion disassembly [58] suggesting that the large isoforms might affect ECM remodeling even if not incorporated into the matrix.

Could this difference in matrix binding and incorporation contribute to the increased ECM in glomerulosclerosis? Based on our results and the findings of others, we propose a model whereby the level and splicing of TN-C play a role in restricting mesangial matrix expansion in the kidney. In normal

glucose conditions, small TN-C isoforms bind to FN and are incorporated into the matrix where they can limit the degree of FN matrix assembly in the glomerulus by controlling FN-syndecan-4 interactions, cell signaling, and contractility. Since collagen IV matrix accumulation depends on the FN matrix [6], TN-C may also indirectly regulate collagen levels in the mesangial matrix. The effects of TN-C on cell-FN interactions, proliferation, and matrix contraction can be rescued by over-expression of syndecan-4 [39,41,43], indicating that the TN-C inhibitory activities are dose-dependent. Accumulation of TN-C in the matrix might have to reach a threshold before inhibition takes effect, essentially providing a TN-C checkpoint. In high glucose conditions, selective expression of larger isoforms could decrease TN-C levels in the matrix such that ECM assembly could proceed without the hypothetical TN-C checkpoint, thus allowing unrestrained assembly and accumulation of FN and collagen IV matrix in the mesangium.

To our knowledge, the differential expression of TN-C isoforms has not been described in the context of diabetic nephropathy and, while our results suggest a correlation between TN-C isoforms and conditions that affect ECM levels, other work suggests a role in the immune response. The immune system is commonly implicated in the pathology of glomerulosclerosis, and T-cell invasion is known to increase the severity of the disease [59]. However, mediators including ECM proteins released by immune cells can have pro- or anti-fibrotic effects [60]. A large isoform of TN-C up-regulated in non-small cell lung cancer was shown to inhibit T-cell proliferation and to reduce production of inflammatory cytokines [61] suggesting that this isoform may be capable of controlling the immune response. A pair of alternatively spliced domains present in TN-C from human and chick but not mouse have been shown to be pro-inflammatory [62] suggesting species-specific effects of TN-C splicing. Thus, while selective up-regulation of a large TN-C isoform in diabetic nephropathy may allow excess ECM deposition, it may also help to limit glomerular damage caused by an over-active T-cell response. Perhaps the functions of TN-C isoforms vary with time such that the initial effect of a large TN-C isoform is protective but as it accumulates in a chronic condition like diabetes, its activities expand to promote a fibrotic response.

Supplementary data to this article can be found online at https://doi.org/10.1016/j.mbplus.2020.100048.

Funding

This research was funded by the Princeton University - University of Geneva Partnership, Sud Cook '39 Fund, and NIH R01 AR073236 (to J.E.S.) and NIH F32 DK109622 post-doctoral fellowship (to M.E.V.).

CRediT authorship contribution statement

Conceptualization (M.E.V; J.B•F; J.E.S); Methodology (M.E.V; J.B•F; M.V, J.E.S); Validation (M.E.V; J.B•F; M.V); Formal analysis (M.E.V; J.B•F; M.V; J.E.S); Investigation (M.E.V; J.B•F; M.V); Resources (M.E.V; J.B•F; M.V); Original Draft writing (M.E.V; J.B•F; J.E.S); Visualization (M.E.V; J.B•F; J.E.S); Supervision (J.E.S); Funding acquisition (M.E.V; J.E.S).

Declaration of competing interest

The authors declare no conflict of interest. The funders had no role in the design of the study; in the collection, analyses, or interpretation of data; in the writing of the manuscript, or in the decision to publish the results.

Acknowledgments

We are grateful to Luqiong Wang for technical assistance. We thank Wei Wang, director of the Genomics Core Facility of the Lewis-Sigler Institute for Integrative Genomics, for RNA-sequencing and data analysis and Saw Kyin, acting director of the Proteomics and Mass Spectrometry Core of the Department of Molecular Biology, for mass spectrometric analyses. We thank Harold Erickson and Ikramuddin Aukhil for providing BHK-HxB cell lines. We also thank members of the Schwarzbauer lab for insightful discussions.

Received 10 June 2020;
Received in revised form 25 August 2020;
Accepted 19 September 2020
Available online 30 September 2020

Keywords:
Diabetic nephropathy;
Extracellular matrix;
Gene expression;
Tenascin-C;
Fibronectin;
Alternative splicing

[1]Equal contributions.

Abbreviations used:
ECM, extracellular matrix; FN, fibronectin; KEGG, Kyoto Encyclopedia of Genes and Genomes; TN-C, tenascin-C; NPNT, nephronectin; DOC, deoxycholate.

References

[1] W.R. Rowley, C. Bezold, Y. Arikan, E. Byrne, S. Krohe, Diabetes 2030: insights from yesterday, today, and future trends, Popul. Health Manag. 20 (2017) 6–12.

[2] V.P. Singh, A. Bali, N. Singh, A.S. Jaggi, Advanced glycation end products and diabetic complications, Korean J Physiol Pharmacol 18 (2014) 1–14.

[3] K. Reidy, H.M. Kang, T. Hostetter, K. Susztak, Molecular mechanisms of diabetic kidney disease, J. Clin. Invest. 124 (2014) 2333–2340.

[4] F.C. Brosius 3rd, New insights into the mechanisms of fibrosis and sclerosis in diabetic nephropathy, Rev. Endocr. Metab. Disord. 9 (2008) 245–254.

[5] A.J. Dixon, J. Burns, M.S. Dunnill, J.O. McGee, Distribution of fibronectin in normal and diseased human kidneys, J. Clin. Pathol. 33 (1980) 1021–1028.

[6] C.G. Miller, A. Pozzi, R. Zent, J.E. Schwarzbauer, Effects of high glucose on integrin activity and fibronectin matrix assembly by mesangial cells, Mol. Biol. Cell 25 (2014) 2342–2350.

[7] A.K. Pastino, T.M. Greco, R.A. Mathias, I.M. Cristea, J.E. Schwarzbauer, Stimulatory effects of advanced glycation endproducts (AGEs) on fibronectin matrix assembly, Matrix Biol. 59 (2017) 39–53.

[8] M.E. Vega, B. Kastberger, B. Wehrle-Haller, J.E. Schwarzbauer, Stimulation of fibronectin matrix assembly by lysine acetylation, Cells 9 (2020) 655.

[9] M. Kato, R. Natarajan, Epigenetics and epigenomics in diabetic kidney disease and metabolic memory, Nat Rev Nephrol 15 (2019) 327–345.

[10] B. Tampe, M. Zeisberg, Chromatin dynamics at the core of kidney fibrosis, Matrix Biol. 68-69 (2018) 194–229.

[11] Y. De Marinis, M. Cai, P. Bompada, D. Atac, O. Kotova, M.E. Johansson, E. Garcia-Vaz, M.F. Gomez, M. Laakso, L. Groop, Epigenetic regulation of the thioredoxin-interacting protein (TXNIP) gene by hyperglycemia in kidney, Kidney Int. 89 (2016) 342–353.

[12] M. Cai, P. Bompada, D. Atac, M. Laakso, L. Groop, Y. De Marinis, Epigenetic regulation of glucose-stimulated osteopontin (OPN) expression in diabetic kidney, Biochem. Biophys. Res. Commun. 469 (2016) 108–113.

[13] G. Sun, M.A. Reddy, H. Yuan, L. Lanting, M. Kato, R. Natarajan, Epigenetic histone methylation modulates fibrotic gene expression, J. Am. Soc. Nephrol. 21 (2010) 2069–2080.

[14] J. Morrison, K. Knoll, M.J. Hessner, M. Liang, Effect of high glucose on gene expression in mesangial cells: upregulation of the thiol pathway is an adaptational response, Physiol. Genomics 17 (2004) 271–282.

[15] M. Liu, W. Lu, Q. Hou, B. Wang, Y. Sheng, Q. Wu, B. Li, X. Liu, X. Zhang, A. Li, H. Zhang, R. Xiu, Gene expression profiles of glucose toxicity-exposed islet microvascular endothelial cells, Microcirculation 25 (2018), e12450, .

[16] M. Stevens, S. Oltean, Alternative splicing in CKD, J. Am. Soc. Nephrol. 27 (2016) 1596–1603.

[17] H.S. Bevan, N.M. van den Akker, Y. Qiu, J.A. Polman, R.R. Foster, J. Yem, A. Nishikawa, S.C. Satchell, S.J. Harper, A.C. Gittenberger-de Groot, D.O. Bates, The alternatively spliced anti-angiogenic family of VEGF isoforms VEGFxxxb in human kidney development, Nephron Physiol 110 (2008) 57–67.

[18] H.J. Baelde, M. Eikmans, P.P. Doran, D.W. Lappin, E. de Heer, J.A. Bruijn, Gene expression profiling in glomeruli from human kidneys with diabetic nephropathy, Am. J. Kidney Dis. 43 (2004) 636–650.

[19] A. Van Vliet, H.J. Baelde, L.J. Vleming, E. de Heer, J.A. Bruijn, Distribution of fibronectin isoforms in human renal disease, J. Pathol. 193 (2001) 256–262.

[20] X. Chen, T.D. Abair, M.R. Ibanez, Y. Su, M.R. Frey, R.S. Dise, D.B. Polk, A.B. Singh, R.C. Harris, R. Zent, A. Pozzi, Integrin alpha1beta1 controls reactive oxygen species synthesis by negatively regulating epidermal growth factor receptor-mediated Rac activation, Mol. Cell. Biol. 27 (2007) 3313–3326.

[21] I. Aukhil, P. Joshi, Y. Yan, H.P. Erickson, Cell- and heparin-binding domains of the hexabrachion arm identified by tenascin expression proteins, J. Biol. Chem. 268 (1993) 2542–2553.

[22] S.W. Wingett, S. Andrews, FastQ Screen: a tool for multi-genome mapping and quality control, F1000Res 7 (2018) 1338.

[23] D. Kim, G. Pertea, C. Trapnell, H. Pimentel, R. Kelley, S.L. Salzberg, TopHat2: accurate alignment of transcriptomes in the presence of insertions, deletions and gene fusions, Genome Biol. 14 (2013) R36.

[24] B.L. Aken, P. Achuthan, W. Akanni, M.R. Amode, F. Bernsdorff, J. Bhai, K. Billis, D. Carvalho-Silva, C. Cummins, P. Clapham, L. Gil, C.G. Girón, L. Gordon, T. Hourlier, S.E. Hunt, S.H. Janacek, T. Juettemann, S. Keenan, M.R. Laird, I. Lavidas, T. Maurel, W. McLaren, B. Moore, D.N. Murphy, R. Nag, V. Newman, M. Nuhn, C.K. Ong, A. Parker, M. Patricio, H.S. Riat, D. Sheppard, H. Sparrow, K. Taylor, A. Thormann, A. Vullo, B. Walts, S.P. Wilder, A. Zadissa, M. Kostadima, F.J. Martin, M. Muffato, E. Perry, M. Ruffier, D.M. Staines, S.J. Trevanion, F. Cunningham, A. Yates, D.R. Zerbino, P. Flicek, Ensembl 2017, Nucleic Acids Res. 45 (2017) D635–d642.

[25] L. Wang, S. Wang, W. Li, RSeQC: quality control of RNA-seq experiments, Bioinformatics 28 (2012) 2184–2185.

[26] S. Anders, P.T. Pyl, W. Huber, HTSeq–a Python framework to work with high-throughput sequencing data, Bioinformatics 31 (2015) 166–169.

[27] M.I. Love, W. Huber, S. Anders, Moderated estimation of fold change and dispersion for RNA-seq data with DESeq2, Genome Biol. 15 (2014) 550.

[28] W. Luo, C. Brouwer, Pathview: an R/bioconductor package for pathway-based data integration and visualization, Bioinformatics 29 (2013) 1830–1831.

[29] M.E. Vega, B. Kastberger, B. Wehrle-Haller, J.E. Schwarzbauer, Stimulation of fibronectin matrix assembly by lysine acetylation, Cells 9 (2020) 655.

[30] I. Wierzbicka-Patynowski, Y. Mao, J.E. Schwarzbauer, Analysis of fibronectin matrix assembly, Curr. Protoc. Cell Biol. (2004) (Chapter 10) Units 10.12.10–10.12.10.

[31] I. Raitman, M.L. Huang, S.A. Williams, B. Friedman, K. Godula, J.E. Schwarzbauer, Heparin-fibronectin interactions in the development of extracellular matrix insolubility, Matrix Biol. 67 (2018) 107–122.

[32] C.G. Miller, Mesangial cell matrix deposition in high glucose as a model of glomerulosclerosis, Ph.D. Thesis Princeton University, 2014.

[33] S. Nakatani, E. Ishimura, K. Mori, S. Fukumoto, S. Yamano, M. Wei, M. Emoto, H. Wanibuchi, M. Inaba, Nephronectin expression in glomeruli of renal biopsy specimens from various kidney diseases: nephronectin is expressed in the mesangial matrix expansion of diabetic nephropathy, Nephron Clin Pract 122 (2012) 114–121.

[34] K.S. Midwood, M. Chiquet, R.P. Tucker, G. Orend, Tenascin-C at a glance, J. Cell Sci. 129 (2016) 4321–4327.

[35] S.P. Giblin, K.S. Midwood, Tenascin-C: form versus function, Cell Adhes. Migr. 9 (2015) 48–82.
[36] C.Y. Chung, L. Zardi, H.P. Erickson, Binding of tenascin-C to soluble fibronectin and matrix fibrils, J. Biol. Chem. 270 (1995) 29012–29017.
[37] W.S. To, K.S. Midwood, Identification of novel and distinct binding sites within tenascin-C for soluble and fibrillar fibronectin, J. Biol. Chem. 286 (2011) 14881–14891.
[38] R. Chiquet-Ehrismann, Y. Matsuoka, U. Hofer, J. Spring, C. Bernasconi, M. Chiquet, Tenascin variants: differential binding to fibronectin and distinct distribution in cell cultures and tissues, Cell. Regul. 2 (1991) 927–938.
[39] K.S. Midwood, L.V. Valenick, H.C. Hsia, J.E. Schwarzbauer, Coregulation of fibronectin signaling and matrix contraction by tenascin-C and syndecan-4, Mol. Biol. Cell 15 (2004) 5670–5677.
[40] A. Joester, A. Faissner, The structure and function of tenascins in the nervous system, Matrix Biol. 20 (2001) 13–22.
[41] W. Huang, R. Chiquet-Ehrismann, J.V. Moyano, A. Garcia-Pardo, G. Orend, Interference of tenascin-C with syndecan-4 binding to fibronectin blocks cell adhesion and stimulates tumor cell proliferation, Cancer Res. 61 (2001) 8586–8594.
[42] K.S. Midwood, J.E. Schwarzbauer, Tenascin-C modulates matrix contraction via focal adhesion kinase- and rho-mediated signaling pathways, Mol. Biol. Cell 13 (2002) 3601–3613.
[43] G. Orend, W. Huang, M.A. Olayioye, N.E. Hynes, R. Chiquet-Ehrismann, Tenascin-C blocks cell-cycle progression of anchorage-dependent fibroblasts on fibronectin through inhibition of syndecan-4, Oncogene 22 (2003) 3917–3926.
[44] N. Nakao, N. Hiraiwa, A. Yoshiki, F. Ike, M. Kusakabe, Tenascin-C promotes healing of Habu-snake venom-induced glomerulonephritis: studies in knockout congenic mice and in culture, Am. J. Pathol. 152 (1998) 1237–1245.
[45] S. Yamada, T. Ichida, Y. Matsuda, Y. Miyazaki, T. Hatano, K. Hata, H. Asakura, N. Hirota, A. Geerts, E. Wisse, Tenascin expression in human chronic liver disease and in hepatocellular carcinoma, Liver 12 (1992) 10–16.
[46] R. Kaarteenaho-Wiik, P. Mertaniemi, E. Sajanti, Y. Soini, P. Pääkkö, Tenascin is increased in epithelial lining fluid in fibrotic lung disorders, Lung 176 (1998) 371–380.
[47] C.S. Lieber, D.G. Weiss, F. Paronetto, Value of fibrosis markers for staging liver fibrosis in patients with precirrhotic alcoholic liver disease, Alcohol. Clin. Exp. Res. 32 (2008) 1031–1039.
[48] K.S. Midwood, G. Orend, The role of tenascin-C in tissue injury and tumorigenesis, J Cell Commun Signal 3 (2009) 287–310.
[49] A.G. Nerlich, E.D. Schleicher, I. Wiest, U. Specks, R. Timpl, Immunohistochemical localization of collagen VI in diabetic glomeruli, Kidney Int. 45 (1994) 1648–1656.
[50] A. Weller, S. Beck, P. Ekblom, Amino acid sequence of mouse tenascin and differential expression of two tenascin isoforms during embryogenesis, J. Cell Biol. 112 (1991) 355–362.
[51] P. Weber, P. Ferber, R. Fischer, K.H. Winterhalter, L. Vaughan, Binding of contactin/F11 to the fibronectin type III domains 5 and 6 of tenascin is inhibited by heparin, FEBS Lett. 389 (1996) 304–308.
[52] C.Y. Chung, H.P. Erickson, Cell surface annexin II is a high affinity receptor for the alternatively spliced segment of tenascin-C, J. Cell Biol. 126 (1994) 539–548.
[53] A. Siri, V. Knäuper, N. Veirana, F. Caocci, G. Murphy, L. Zardi, Different susceptibility of small and large human tenascin-C isoforms to degradation by matrix metalloproteinases, J. Biol. Chem. 270 (1995) 8650–8654.
[54] H. Ge, J.L. Manley, A protein factor, ASF, controls cell-specific alternative splicing of SV40 early pre-mRNA in vitro, Cell 62 (1990) 25–34.
[55] A.R. Krainer, G.C. Conway, D. Kozak, The essential pre-mRNA splicing factor SF2 influences 5′ splice site selection by activating proximal sites, Cell 62 (1990) 35–42.
[56] M.A. Jensen, J.E. Wilkinson, A.R. Krainer, Splicing factor SRSF6 promotes hyperplasia of sensitized skin, Nat. Struct. Mol. Biol. 21 (2014) 189–197.
[57] S. Saoncella, F. Echtermeyer, F. Denhez, J.K. Nowlen, D.F. Mosher, S.D. Robinson, R.O. Hynes, P.F. Goetinck, Syndecan-4 signals cooperatively with integrins in a rho-dependent manner in the assembly of focal adhesions and actin stress fibers, Proc. Natl. Acad. Sci. U. S. A. 96 (1999) 2805–2810.
[58] J.E. Murphy-Ullrich, V.A. Lightner, I. Aukhil, Y.Z. Yan, H.P. Erickson, M. Höök, Focal adhesion integrity is downregulated by the alternatively spliced domain of human tenascin, J. Cell Biol. 115 (1991) 1127–1136.
[59] E. Galkina, K. Ley, Leukocyte recruitment and vascular injury in diabetic nephropathy, J. Am. Soc. Nephrol. 17 (2006) 368–377.
[60] M. Mack, Inflammation and fibrosis, Matrix Biol. 68-69 (2018) 106–121.
[61] K. Parekh, S. Ramachandran, J. Cooper, D. Bigner, A. Patterson, T. Mohanakumar, Tenascin-C, over expressed in lung cancer down regulates effector functions of tumor infiltrating lymphocytes, Lung Cancer 47 (2005) 17–29.
[62] S.P. Giblin, A. Schwenzer, K.S. Midwood, Alternative splicing controls cell lineage-specific responses to endogenous innate immune triggers within the extracellular matrix, Matrix Biol. (2020)https://doi.org/10.1016/j.matbio.2020.06.003.